Structural Studies of LNA:RNA Duplexes by NMR: Conformations and Implications for RNase H Activity**

Kent Bondensgaard,[a] Michael Petersen,[a] Sanjay K. Singh,[b] Vivek K. Rajwanshi,[b] Ravindra Kumar,[b] Jesper Wengel,[b] and Jens Peter Jacobsen*[a]

Abstract: We have used NMR and CD spectroscopy to study the conformations of modified oligonucleotides (locked nucleic acid, LNA) containing a conformationally restricted nucleotide ($\mathbf{T^L}$) with a 2′-*O*,4′-*C*-methylene bridge. We have investigated two LNA:RNA duplexes, d(CTGA$\mathbf{T^L}$ATGC):r(GCAUAUCAG) and d(C$\mathbf{T^L}$GA$\mathbf{T^L}$A$\mathbf{T^L}$GC):r(GCAUAUCAG), along with the unmodified DNA:RNA reference duplex. Increases in the melting temperatures of $+9.6\,^{\circ}C$ and $+8.1\,^{\circ}C$ per modification relative to the unmodified duplex were observed for these two LNA:RNA sequences. The three duplexes all adopt right-handed helix conformations and form normal Watson–Crick base pairs with all the bases in the *anti* conformation. Sugar conformations were determined from measurements of scalar coupling constants in the sugar rings and distance information derived from $^1H-^1H$ NOE measurements; all the sugars in the RNA strands of the three duplexes adopt an *N*-type conformation (*A*-type structure), whereas the sugars in the DNA strands change from an equilibrium between *S*- and *N*-type conformations in the unmodified duplex towards more of the *N*-type conformation when modified nucleotides are introduced. The presence of three modified $\mathbf{T^L}$ nucleotides induces drastic conformational shifts of the remaining unmodified nucleotides of the DNA strand, changing all the sugar conformations except those of the terminal sugars to the *N* type. The CD spectra of the three duplexes confirm the structural changes described above. On the basis of the results reported herein, we suggest that the observed conformational changes can be used to tune LNA:RNA duplexes into substrates for RNase H: Partly modified LNA:RNA duplexes may adopt a duplex structure between the standard *A* and *B* types, thereby making the RNA strand amenable to RNase H-mediated degradation.

Keywords: antisense agents · enzyme catalysis · locked nucleic acids · nucleic acids · RNA

Introduction

Since the recognition of the therapeutic potential of antisense technology,[1, 2] interest in this research area has grown and a vast number of chemically modified oligonucleotides have been prepared. Several requirements must be fulfilled by a potential antisense oligonucleotide. Among these are enhanced stability under physiological conditions, including stability towards cellular nucleases (a property which neither DNA nor RNA possesses), effective delivery to cells in vivo, low toxicity, and high affinity and sequence selectivity towards cognate RNA.[1–7] Furthermore, the antisense efficiency is enhanced if the duplex formed by hybridization with the target RNA is amenable to RNase H-mediated degradation.[8, 9]

In spite of an extensive search, the perfect antisense candidate meeting all demands has so far remained elusive. A most promising nucleotide analogue recently introduced is LNA (Scheme 1), a conformationally restricted nucleotide containing a 2′-*O*,4′-*C*-methylene bridge. X-ray crystallography, NMR spectroscopy and molecular modelling studies

[a] Ass. Prof. Dr. J. P. Jacobsen, M.Sc. K. Bondensgaard, M.Sc. M. Petersen
Department of Chemistry, University of Southern Denmark Odense University, DK-5230 Odense M (Denmark)
Fax: (+45) 6615-8780
E-mail: jpj@chem.sdu.dk

[b] Dr. S. K. Singh, Dr. V. K. Rajwanshi, Dr. R. Kumar, Prof. J. Wengel
Center for Synthetic Bioorganic Chemistry
Department of Chemistry, University of Copenhagen
Universitetsparken 5, DK-2100 Copenhagen (Denmark)

[**] **Abbreviations**: CD, circular dichroism; DNA, deoxyribose nucleic acid; DQF COSY, double-quantum filtered correlation spectroscopy; dsDNA, double-stranded DNA; E-BURP, excitation band-selective pulse with uniform response and pure phase; EDTA, ethylenediaminetetraacetic acid; HSQC, heteronuclear single-quantum coherence spectroscopy; LNA, locked nucleic acid; MARDIGRAS, matrix analysis of relaxation for discerning the geometry of an aqueous structure; NMR, nuclear magnetic resonance; NOE, nuclear Overhauser effect; NOESY, nuclear Overhauser effect spectroscopy; RANDMARDI, randomized MARDIGRAS; TOCSY, total correlation spectroscopy.

  0947-6539/00/0615-2687 $ 17.50+.50/0

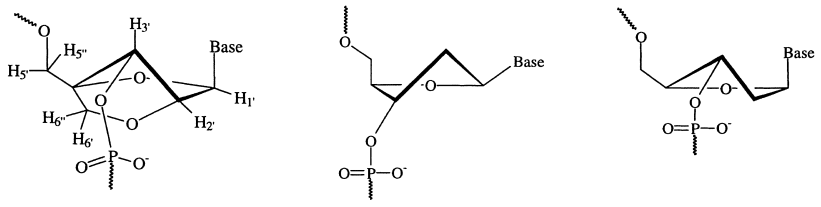

LNA ***C2'-endo* (*S* - type)** ***C3'-endo* (*N* - type)**

Scheme 1. The conformationally locked nucleotide analogue LNA, and *S*- and *N*-type sugar conformations.

have shown that LNA is locked in an *N*-type conformation with a pseudorotation angle of $P = 17^\circ$ and can thus be classified as an RNA mimic.[10–16] LNA (the term "LNA" is used in the following to denote an oligonucleotide containing one or more 2′-*O*,4′-*C*-methylene-linked bicyclic ribonucleoside monomers) has shown unprecedented helical thermal stability when hybridized to either complementary DNA or RNA without reduced sequence selectivity. Increases in the melting temperature ranging from $\Delta T_m = +4.0\,^\circ C$ to $+9.3\,^\circ C$ per LNA nucleotide compared with unmodified duplexes have been observed.[10–13] LNA is easily incorporated into oligonucleotides by standard procedures and has shown stability towards 3′-exonucleolytic degradation. Preliminary experiments suggest that LNA is able to recognize a mixed-sequence segment of dsDNA by strand invasion.[17] In addition, fluorescein-labelled LNA can be effectively delivered into living MCF-7 breast cancer cells by Lipofectin-mediated transfection.[17] These properties make LNA extremely interesting as a potential antisense and/or antigen molecule.

In general, the conformations of the flexible deoxyribose/ribose rings determine the overall structure of a nucleic acid duplex. Duplexes of the *A*-type structure contain nucleotides with an *N*-type (C3′-*endo*, Scheme 1) sugar conformation, while *B*-type duplexes contain nucleotides with an *S*-type (C2′-*endo*, Scheme 1) sugar conformation.[18, 19] In general, *N*-type sugars are described by a pseudorotation angle *P* between -90° and 90°, while for *S*-type sugars *P* is between 90° and 270°.[20, 21] Due to the low energy barrier between these two conformations (≈ 2 kcal mol^{-1}[22, 23]), nucleotides are not trapped completely in either conformation but rather exist in a fast equilibrium between these (the *N*,*S* two-state model).[20, 21]

Recently, we reported sugar conformations of an LNA 9-mer single-stranded deoxyoligonucleotide as well as three 9- and 10-mer LNAs hybridized to unmodified DNA.[24–26] We suggested that the enhanced thermal stabilities of LNA:DNA duplexes were caused by a local organization of the phosphate backbone due to the locked C3′-*endo* conformation of the LNA nucleotides. We then embarked on the characterization of two LNA:RNA duplexes (containing one and three modifications) along with the unmodified DNA:RNA reference sequence (Scheme 2) in order to investigate whether the RNA-mimicking character of LNA yields LNA:RNA duplexes with structures that are susceptible to RNase H activity while still retaining the favourable features of this modified nucleotide.

```
                  1   2   3   4   5   6   7   8   9
1   5' - d(  C   T   G   A   T   A   T   G   C  ) - 3'
    3' - r(  G   A   C   U   A   U   A   C   G  ) - 5'
            18  17  16  15  14  13  12  11  10

2   5' - d(  C   T   G   A   T^L A   T   G   C  ) - 3'
    3' - r(  G   A   C   U   A   U   A   C   G  ) - 5'

3   5' - d(  C   T^L G   A   T^L A   T^L G   C  ) - 3'
    3' - r(  G   A   C   U   A   U   A   C   G  ) - 5'
```

Scheme 2. The unmodified DNA:RNA reference sequence **1** and the LNA:RNA duplexes **2** and **3** containing one and three modifications, respectively. $\mathbf{T}^L$ denotes an LNA thymine nucleotide.

ments of scalar coupling constants in the sugar rings and distance information was derived from $^1H-^1H$ nuclear Overhauser effect (NOE) measurements.

Results

Thermal stabilities: The thermal stabilities of the modified LNA:RNA duplexes were determined and compared with that of the unmodified reference sequence (Table 1). Sharp monophasic transitions were obtained with hyperchromicities of 1.2–1.3. No indications of biphasic transitions were detected. These results emphasize the remarkable thermal stability displayed by LNA hybridized with either complementary DNA or RNA.[10–13] For the LNA:RNA duplexes containing one and three modifications we observed increases in the melting temperature of $+9.6$ and $+8.1\,^\circ C$ per modification, respectively, relative to the reference duplex.

Table 1. Melting temperatures of LNA:RNA duplexes compared with the unmodified duplex.[a]

Duplex	Number of modifications	T_m [°C]	ΔT_m per mod. [°C]
1	none	27.2	–
2	one	36.8	9.6
3	three	51.6	8.1

[a] T_m is the melting temperature and ΔT_m the increase in melting temperature compared with that of the unmodified DNA:RNA duplex.

Circular dichroism spectra: The CD spectra of the three duplexes are shown in Figure 1. The unmodified reference duplex **1** shows CD features intermediate between *A*- and *B*-type structures. The spectrum displays a positive band at 267 nm and a less intense negative band around 245 nm. Both bands are indicative of a *B*-type structure, but in a pure *B*-type

0947-6539/00/0615-2688 $ 17.50+.50/0 *Chem. Eur. J.* **2000**, *6*, No. 15

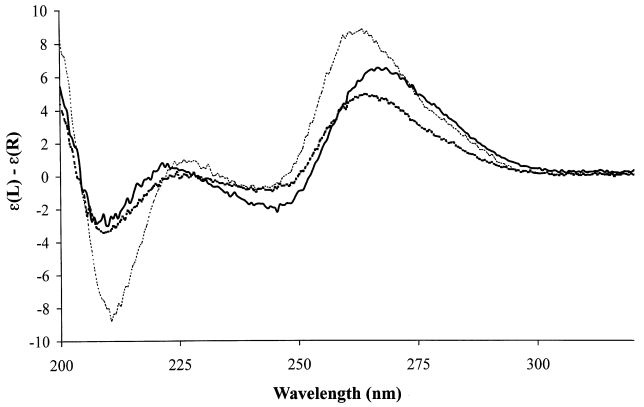

Figure 1. The CD spectra of the unmodified duplex **1** (——), the d(CTGA**T**^{L}ATGC):r(GCAUAUCAG) duplex **2** (----), and the d(C**T**^{L}GA**T**^{L}A**T**^{L}GC):r(GCAUAUCAG) duplex **3** (••••).

structure they have approximately equal intensity. A negative band at 210 nm is also observed. An intense negative band at this wavelength is characteristic for an *A*-type structure, but in the spectrum of duplex **1** the observed band is rather weak.

The CD spectrum of the duplex **2**, with one LNA modification, is very similar to that of duplex **1**. However, there are small differences: The band in the region 260–270 nm is blue-shifted to 264 nm and is approximately 30% less intense in duplex **2** than in duplex **1**. The negative band at 245 nm is also less intense in duplex **2**; instead the band at 210 nm has gained a little intensity. Thus, as a whole, duplex **2** displays the same features as duplex **1**, but has more *A*-type structure characteristics.

More pronounced changes are observed in the CD spectrum of the duplex **3**, with three LNA modifications. This spectrum has exclusively *A*-type conformation characteristics, with a band at 263 nm, which is more intense than the corresponding band observed for duplexes **1** and **2**, and a very intense band at 210 nm.

In conclusion, duplexes **1** and **2** display CD features intermediate between *A*- and *B*-type structures, with duplex **2** having slightly more *A*-type structure characteristics than duplex **1** while duplex **3** exhibits exclusively *A*-type structure characteristics.

Spectral analysis: The 1-D ^{1}H NMR spectra of the three samples contain sharp lines from the expected LNA/DNA:RNA duplexes. No signs of any minor forms were observed for duplexes **2** and **3**. However, the NOESY spectrum of duplex **1** contains additional weak resonances at 25 °C probably stemming from traces of single-stranded DNA and RNA.

The NOESY spectra of the duplexes display the characteristic features of a right-handed double helix with all the nucleobases in the *anti* conformation. The assignment of protons in the duplexes was performed by standard methods.[27–30] The NOESY spectra with short mixing times allowed unambiguous assignment of the H2′ and H2″ resonances of the deoxyribose nucleotides and the H2′ resonances of the ribose and LNA nucleotides (Figure 2). The H6′ and H6″ resonances in the C2′,C4′ linker of the LNA nucleotides were assigned by their strong intranucleotide cross-peaks to H1′

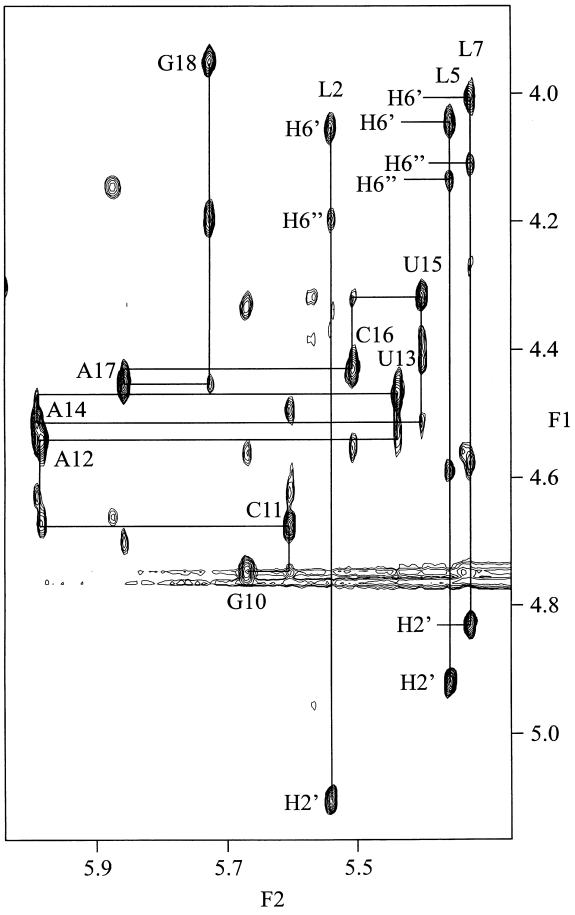

Figure 2. The H1′ to H2′ region of the 60 ms NOESY spectrum of the d(C**T**^{L}GA**T**^{L}A**T**^{L}GC):r(GCAUAUCAG) duplex obtained at 750 MHz. The solid line indicates the important sequential connectivity pathway from H2′(n)–H1′(n)–H2′($n+1$) of the RNA strand as well as some of the assignments related to the modified nucleotides in the LNA strand.

(Figure 2). The NOESY spectra recorded in H_2O display the normal Watson–Crick connectivity pattern. We do observe some NOE's between C9 and G10 and between G1 and G18 that cannot comply with Watson–Crick base-pairing. These terminal base pairs seem to exist in an equilibrium between Watson–Crick base-pairing and some alternative base-pairing scheme.

A selection of chemical shift values for the three duplexes is given in Table 2. As expected, large chemical shift differences among the three duplexes are observed for the modified nucleotides: for example, the H2′ protons shift ≈2.5 ppm downfield and the H1′ protons shift ≈0.5 ppm upfield. In addition, minor chemical shift differences are found near the modification sites in the DNA strand. However, in duplex **3** almost all H3′ protons are shifted ≈0.2 ppm upfield relative to duplex **1**. An identical pattern is observed for the H3′ proton in the modified nucleotide and for the 3′-flanking nucleotide in duplex **2**. This may correlate with sugar conformations (C2′-*endo* versus C3′-*endo*) as H3′ experiences a large change in position on going from a C2′-*endo* conformation to a C3′-*endo* conformation. In the RNA strand virtually identical chemical shift values of the three duplexes suggest that this strand is largely unperturbed upon introduction of the modified LNA nucleotides.

Table 2. Chemical shift (δ) values of **1, 2** and **3.**[a]

	H1′	H2′	H2′	H3′	H6/H8	H5/H2/CH_3	H1/H3
C1	5.90/5.94/5.85	2.42/2.41/2.62	2.68/2.69/2.75	4.68/4.69/4.64	7.98/7.98/8.00	6.02/6.04/5.96	
T^{L}2/T2	6.17/6.19/5.52	2.46/2.46/5.08	2.74/2.74/ –[b]	4.97/4.98/4.77	7.71/7.70/7.54	1.73/1.73/1.68	13.79/ – /13.83
G3	5.89/5.89/6.03	2.66/2.64/2.67	2.77/2.77/2.79	4.99/5.01/4.81	7.77/7.75/7.83		11.91/11.93/11.69
A4	6.22/6.23/6.12	2.60/2.81/2.71	2.87/2.86/2.80	4.86/4.88/4.67	7.93/7.98/7.73	7.65/7.64/7.56	
T^{L}5/T5	5.88/5.32/5.34	2.27/4.74/4.89	2.60/ –[b] / –[b]	4.84/4.56/4.56	7.24/6.94/6.99	1.35/1.40/1.26	13.19/12.23/13.29
A6	6.21/6.23/6.21	2.51/2.53/2.73	2.84/2.79/2.80	4.88/4.78/4.74	7.98/7.96/8.06	7.20/7.15/7.06	
T^{L}7/T7	5.92/6.01/5.30	2.26/2.34/4.80	2.54/2.61/ –[b]	4.86/4.85/4.56	7.20/7.47/7.04	1.25/1.17/1.21	13.37/13.42/13.56
G8	5.99/6.02/6.05	2.48/2.49/2.52	2.68/2.70/2.62	4.88/4.90/4.72	7.62/7.67/7.73		12.43/12.49/12.55
C9	6.19/6.22/6.07	2.09/2.11/2.10	2.21/2.22/2.26	4.48/4.50/4.39	7.35/7.38/7.52	5.14/5.18/5.21	
G10	5.64/5.72/5.65	4.76/4.81/4.72		4.54/ – /4.53	7.98/8.05/8.02		– / – / –
C11	5.54/5.59/5.58	4.66/4.69/4.65		4.55/4.59/4.60	7.78/7.81/7.86	5.32/5.38/5.31	
A12	5.94/5.98/5.96	4.53/4.58/4.52		4.66/4.65/4.64	8.11/8.11/8.07	7.36/7.43/7.29	
U13	5.42/5.41/5.42	4.55/4.52/4.44		4.49/4.50/4.52	7.64/7.59/7.56	5.17/5.25/5.09	13.19/13.34/13.12
A14	5.94/5.93/5.97	4.48/4.50/4.49		4.58/4.55/4.60	8.12/8.10/8.13	6.98/6.90/7.02	
U15	5.36/5.40/5.38	4.28/4.31/4.29		4.38/4.39/4.36	7.64/7.59/7.52	5.00/4.92/4.93	13.87/13.57/13.84
C16	5.52/5.55/5.49	4.41/4.41/4.41		4.55/4.58/4.53	7.91/7.92/7.81	5.62/5.63/5.55	
A17	5.84/5.85/5.83	4.41/4.42/4.43		4.68/4.70/4.68	8.05/8.07/7.99	7.34/7.35/7.07	
G18	5.73/5.76/5.71	3.96/3.95/3.92		4.23/4.42/4.16	7.44/7.46/7.27		– / – / –

[a] The first number in each cell corresponds to the value of duplex **1**, the second to duplex **2** and the third to duplex **3**. The values are given at 25 °C relative to HOD ($\delta = 4.78$). The protons in the C2′,C4′ linker have the following chemical shift values: **T**^{L}5 H6′/H6″: $\delta = 4.12/4.18$ in duplex **2** and **T**^{L}2 H6′/H6″: 4.03/4.17; **T**^{L}5 H6′/H6″: 4.02/4.11; **T**^{L}7 H6′/H6″: 3.98/4.09 in duplex **3**. [b] Proton missing owing to the 2′-*O*,4′-*C*-linker.

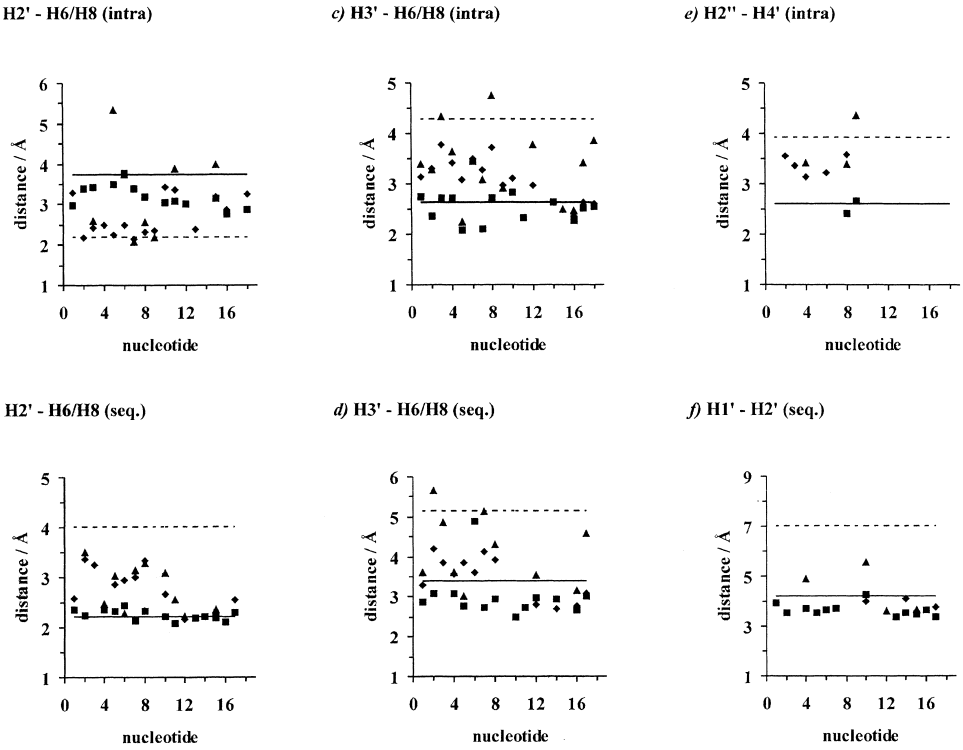

Figure 3. A selection of distances returned by MARDIGRAS for the unmodified duplex **1** (◆), the d(CTGA**T**^{L}ATGC):r(GCAUAUCAG) duplex **2** (▲), and the d(C**T**^{L}GA**T**^{L}A**T**^{L}GC):r(GCAUAUCAG) duplex **3** (■) together with the average interproton distances in canonical *A*-type (——) and *B*-type helices (- - - -). The distances are grouped into intranucleotide (intra) and internucleotide (sequential) distances (seq.).

Interproton distances: Some distances descriptive of *A*-type versus *B*-type helices returned by MARDIGRAS[31, 32] are plotted in Figure 3 together with the average interproton distances in canonical *A*-type and *B*-type helices. The three intranucleotide distances plotted (H2′ – H6/H8, H3′ – H6/H8 and H2″ – H4′) describe the conformation of individual nucleotides. In the unmodified reference duplex **1**, the distances in the RNA strand comply reasonably well with an *A*-type structure, that is, the nucleobase in the *anti* conformation and a C3′-*endo* sugar conformation. In the DNA strand, however, the situation is more complex since the distances indicate a structure between the *A* and *B* types; this is in accordance with the literature.[28] A similar pattern is displayed by duplex **2** except for the modified nucleotide, for which the observed distances reflect the locked *N*-type sugar conformation of this nucleotide. In addition, a distance of $\approx$3.7 Å between the H2′ and H6/H8 protons of A6, the nucleotide flanking the modification in the 3′-direction,

0947-6539/00/0615-2690 $ 17.50+.50/0 *Chem. Eur. J.* **2000**, *6*, No. 15

indicates an *N*-type sugar conformation of this nucleotide. Unfortunately, due to spectral overlap neither the distance between the H3′ and H6/H8 protons nor that between the H2″ and H4′ protons could be extracted to support this observation. All the distances in A4, the nucleotide flanking the modification in the 5′-direction, reflect a structure intermediate of the *A* and *B* type. In duplex **3**, distances returned by MARDIGRAS indicate an *N*-type sugar conformation of all nucleotides in both the RNA and the DNA strand, but the H2′–H6/H8 distances are slightly shorter than in the *A*-type structure. However, due to the r^{-6} averaging of the NOE, even a small population of a *B*-like structure, with a short H2′–H6/H8 distance, would bias the calculation toward the shorter distance.[33]

The three internucleotide distances plotted (H2′(*n*)–H6/H8(*n*+1), H3′(*n*)–H6/H8(*n*+1) and H2′(*n*)–H1′(*n*+1)) display the same features as the intranucleotide distances. With all three duplexes, distances in the RNA strand reflect an overall *A*-type structure. Likewise, the distances of the DNA strand in duplexes **1** and **2** indicate a structure intermediate of the *A* and *B* type. The only exception is in the vicinity of the LNA modification in duplex **2**, where several sequential distances between the nucleotides A4, **T^{L}**5 and A6 agree with a local *A*-type structure such as H2′(A4)–H6/H8(**T^{L}**5) and H3′(**T^{L}**5)–H6/H8(A6). In duplex **3**, the sequential distances in the DNA strand match an *A*-type structure, as do the intranucleotide distances.

Furanose ring conformations: All nucleotides in the RNA strands, along with the LNA nucleotides, are found in an *N*-type conformation; this is shown by the absence of cross-peaks between the H1′ and H2′ protons of these nucleotides in the DQF COSY spectra due to cancellation of lines ($J_{H1'H2'}$ < 2 Hz). A weak cross-peak between H1′ and H2′ of G18 in duplex **3** is probably due to end effects.

The selective DQF COSY spectra of duplexes **1**, **2** and **3** are shown in Figure 4. CHEOPS simulations[34] of the H1′ to H2′/H2″ region of the DQF COSY spectra returned values that correlate well with the experimental spectra. Simulation of A4 and A6 in duplex **2** by CHEOPS was impossible owing to severe spectral overlap for these residues. In the case of duplex **3**, the lack of cross-peaks between H1′ and H2′ made any simulation impossible for all nucleotides except C1 and C9. However, the absence of these cross-peaks was taken as an indication of *N*-type conformations similar to the those in the ribonucleotide. The coupling constants calculated by CHEOPS, together with estimated uncertainties, were used as input for RANDPSEUROT.[24] The coupling constants obtained are given in Table 3. In addition, the fractions of *N*-type sugar conformation and pseudorotation angles calculated by means of RANDPSEUROT are shown in Table 4.

The use of a two-state model in PSEUROT[35] to calculate the sugar pucker from the values of the coupling constants obtained by CHEOPS is well justified. However, we did try to calculate the sugar pucker by using only one conformation in PSEUROT. The results of these PSEUROT calculations are illustrated in Figure 5. A part of the experimental DQF COSY spectrum of the unmodified duplex **1** is shown in Figure 5a. This spectrum was simulated by CHEOPS to yield the experimental values of the coupling constants. The theoretical values of the coupling constants that gave the best fit to the experimental values were obtained by iterative fitting of the sugar conformations by RANDPSEUROT. The theoretical values thus gained were subsequently used by CHEOPS to back-calculate the theoretical DQF COSY spectra in Figure 5b and 5c. The calculation by RAND-

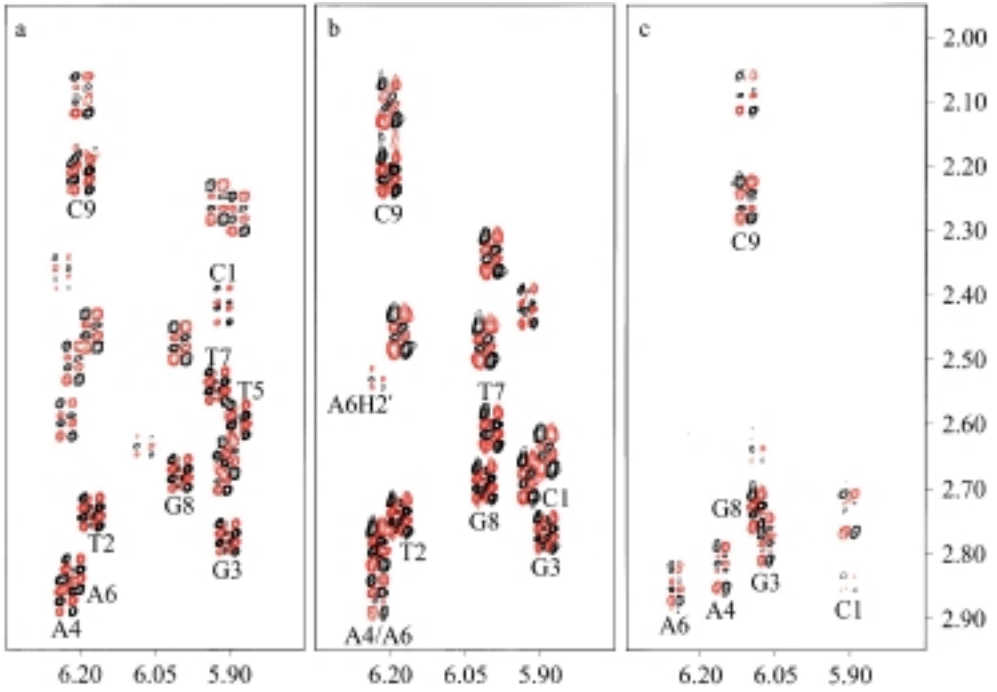

Figure 4. The H1′ to H2′/H2″ region of the selective DQF COSY spectra of the duplexes obtained at 500 MHz. a) Spectrum of the unmodified duplex **1**; b) spectrum of the d(CTGA**T^{L}**ATGC):r(GCAUAUCAG) duplex **2**; c) spectrum of the d(C**T^{L}**GA**T^{L}**A**T^{L}**GC):r(GCAUAUCAG) duplex **3**.

Table 3. Coupling constants (J, in Hz) for the deoxyribose protons in **1, 2** and **3**.[a]

	Duplex **1**				Duplex **2**				Duplex **3**			
	$J_{1'2'}$	$J_{1'2''}$	$J_{2'3'}$	$J_{2''3'}$	$J_{1'2'}$	$J_{1'2''}$	$J_{2'3'}$	$J_{2''3'}$	$J_{1'2'}$	$J_{1'2''}$	$J_{2'3'}$	$J_{2''3'}$
C1	3.9	6.6	5.9	6.4	4.0	6.5	5.3	5.2	4.2	6.0	6.2	7.7
T^{L}2/T2	7.5	6.6	4.7	1.5	8.5	6.0	4.7	1.1	–[d]	–[e]	–[d]	–[e]
G3	7.9	5.5	5.3	2.2	8.2	5.3	5.2	2.3	–[c]	–[c]	–[c]	–[c]
A4	5.6	6.3	5.2	3.4	–[b]	–[b]	–[b]	–[b]	–[c]	–[c]	–[c]	–[c]
T^{L}5/T5	6.8	6.4	5.7	2.6	–[d]	–[e]	–[d]	–[e]	–[d]	–[e]	–[d]	–[e]
A6	6.7	6.3	4.9	2.6	–[b]	–[b]	–[b]	–[b]	–[c]	–[c]	–[c]	–[c]
T^{L}7/T7	8.0	6.6	5.7	1.7	6.5	6.2	4.0	2.0	–[d]	–[e]	–[d]	–[e]
G8	7.8	6.6	4.2	1.8	7.9	5.8	4.4	1.9	–[c]	–[c]	–[c]	–[c]
C9	7.0	6.9	6.6	2.8	6.7	6.6	6.4	1.5	6.4	4.6	5.4	5.8

[a] The coupling constants were derived from the H1′-H2′/H2″ cross-peaks in the selective DQF COSY spectra by means of CHEOPS. The $J_{2'2''}$ coupling constants were fixed at -15 Hz in all CHEOPS simulations. [b] A4 and A6 in duplex **2** could not be simulated owing to spectral overlap. [c] G3, A4, A6 and G8 in duplex **3** could not be simulated owing to absence of the H1′–H2′ cross-peaks caused by cancellation resulting from a small value of $J_{1'2'}$. [d] The LNA nucleotides were not included in the CHEOPS calculations because of the locked conformation. [e] Coupling constant missing because of the 2′-*O*,4′-*C*-linker.

Table 4. Deoxyribose conformations in **1, 2** and **3**.[a]

	Duplex **1**			Duplex **2**			Duplex **3**		
	% *N*	P_N[b]	P_S[b]	% *N*	P_N[b]	P_S[b]	% *N*	P_N[b]	P_S[b]
C1	64 (10)	−10 (25)	169 (39)	56 (10)	−16 (24)	183 (28)	47 (8)	−16 (12)	152 (12)
T^{L}2/T2	16 (12)	–	179 (24)	12 (11)	–	175 (20)	100	17[c]	–
G3	23 (10)	–	162 (21)	20 (9)	–	161 (20)	> 90[d]	–	–
A4	38 (11)	−15 (50)	182 (27)	–[e]	–[e]	–[e]	> 90[d]	–	–
T^{L}5/T5	31 (13)	4 (75)	170 (34)	100	17[c]	–	100	17[c]	–
A6	27 (12)	–	179 (24)	> 90[d]	–	–	> 90[d]	–	–
T^{L}7/T7	20 (14)	–	164 (34)	21 (12)	–	189 (17)	100	17[c]	–
G8	15 (11)	–	184 (18)	17 (10)	–	175 (17)	> 90[d]	–	–
C9	36 (19)	39 (76)	156 (51)	27 (18)	–	166 (47)	70 (10)	−7 (22)	148 (38)

[a] Deoxyribose ring conformations derived from the coupling constants determined with RANDPSEUROT. A two-state model was used and the puckering amplitudes were fixed at 36° in the PSEUROT calculations. The standard deviations are given in parentheses. [b] If the mole fraction of the conformer was below 30% the pseudorotation angle was not considered to be determined with sufficient accuracy. [c] The values of P_N for the LNA nucleotides were taken from Obika et al.[15] [d] The nucleotides for which the H1′–H2′ cross-peak was absent owing to cancellation of lines were considered to be in an *N*-type conformation with a purity above 90%. [e] No coupling constants were determined for A4 in duplex **2** because of spectral overlap.

PSEUROT assumed a two-state model in the case of Figure 5b, whereas a one-state model was assumed in the case of Figure 5c. On inspection, the simulated spectrum from the two-state model resembles the experimental spectrum closely, unlike the spectrum obtained by the one-state model, which deviates significantly. Furthermore, the fitting procedure of PSEUROT in the one-state model converged very badly. Consequently, we disregard the possibility that only a single sugar conformer exists. The two-state model yielded good convergence in the PSEUROT calculations with the results given in Table 3.

The deoxyribose nucleotides in duplex **1** are predominantly in an *S*-type conformation, but with larger fractions of *N*-type sugar conformation than observed in DNA:DNA duplexes. In duplex **2**, the sugar conformations analysed are nearly identical to the conformations in duplex **1** except for the modified LNA nucleotide. The two nucleotides flanking the modification in duplex **2** were not thoroughly analysed because of the overlap problem. However, absence of the H1′–H2′ cross-peak for A6, the nucleotide flanking the LNA modification to the 3′-side, indicates an *N*-type conformation for this nucleotide. All sugars in duplex **3** adopt an *N*-type conformation exclusively, except the terminal nucleotides C1 and C9, which have an appreciable fraction of *S*-type conformation (e.g. for C1: 53% *S*-type conformation).

Discussion

Structure: The three duplexes all adopt a right-handed helix conformation. All bases are in the *anti* conformation and form normal Watson–Crick base pairs. The CD spectrum of the unmodified reference duplex **1** suggests a structure intermediate of the *A* and *B* type. This conclusion is further supported by the NMR data with both the derived interproton distances and the sugar conformations showing that the RNA strand has an overall *A*-type structure whereas the DNA strand has a structure between the *A* and *B* types. Furthermore, the larger fraction of *S*-type than *N*-type sugar conformations in the DNA strand indicates a structure closer to the *B* type than the *A* type for this strand, but the fraction of *N*-type conformations is still somewhat larger than normally observed for DNA:DNA duplexes.

In duplexes **2** and **3**, containing one and three LNA modifications respectively, the derived distances and sugar conformations of the RNA strands are almost identical to those in duplex **1**. This shows that the *A*-type structure of the RNA strand is practically unperturbed upon introduction of the LNA nucleotides in the DNA strand. This is also reflected in the close resemblance of the chemical shift values for the RNA strands in the three duplexes. With the DNA strand, the situation is quite different. Extensive changes in conformation

0947-6539/00/0615-2692 $ 17.50+.50/0 *Chem. Eur. J.* **2000**, *6*, No. 15

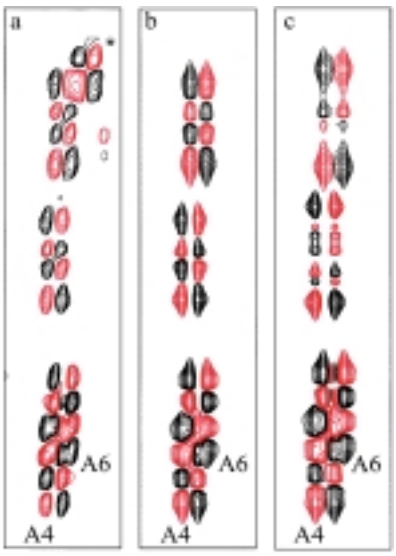

Figure 5. A part of the experimental and simulated selective DQF COSY spectra of the unmodified d(CTGATATGC):r(GCAUAUCAG) duplex **1**. The experimental spectrum obtained at 500 MHz is shown in a). This spectrum was simulated by CHEOPS to yield the experimental values of the coupling constants. The theoretical values of the coupling constants that gave the best fit to the experimental values were obtained by iterative fitting of the sugar conformations by RANDPSEUROT. The theoretical values obtained were subsequently used by CHEOPS to back-calculate the theoretical DQF COSY spectra in b) and c). In the case of b) a two-state model was used in the RANDPSEUROT calculations giving the *N*/*S* equilibrium shown in Table 4. In the case of c) a one-state model was used in the RANDPSEUROT calculations giving single sugar conformations with $P = 78^\circ$ for A4 and $P = 89^\circ$ for A6. The asterisk in a) denotes an overlapping cross-peak that was not used in the simulations.

are observed with the change from no to three modifications. As mentioned above, the DNA strand in the unmodified duplex **1** has an intermediate structure that is closest to a *B*-type structure. When the locked nucleotide $\mathbf{T^L}$5 is introduced into the DNA strand of duplex **2**, several conformational changes are induced. The nucleotide A6, flanking the modification on the 3′-side, adopts an *N*-type conformation (> 90 % *N* type) in contrast to the corresponding nucleotide in duplex **1**, which possesses only 27 % *N*-type conformation. A similar pattern is observed in the derived intranucleotide distances. The intranucleotide H2′ – H6/H8 distance for A6 in duplex **2** indicates an *A*-type structure. With A4, overlap unfortunately precluded any analysis of the sugar conformation of the nucleotide. However, close resemblance between the derived intranucleotide distances of A4 in duplexes **1** and **2** suggests only minor changes in the conformation of this nucleotide. In both duplexes **1** and **2**, the derived distances along with the sugar conformation of A4 in duplex **1** (38 % *N* type) agree with a structure between the *A* and *B* type. On the basis of several internucleotide distances matching an overall *A*-type conformation among A4, $\mathbf{T^L}$5 and A6 in duplex **2**, we estimate that a shift of the overall helix conformation in this region towards an overall *A* type occurs due to the presence of the LNA nucleotide.

In summary, the LNA nucleotide induces a change in the structure of the DNA strand towards an *A* type. However, this effect is entirely local; only the nucleotides flanking the modification are affected (most pronounced for the nucleotide following in the C3′-direction). Similar changes, although to a smaller extent, have also been observed for LNA nucleotides in ssDNA and dsDNA.[24] When three modifications are introduced, in duplex **3**, both sugar conformations and interproton distances of the DNA strand are peculiar to an overall *A*-type structure. All nucleotides except the terminal ones have *N*-type conformations (> 90 % *N* type) and both inter- and intranucleotide distances are consistent with an overall *A*-type structure. Thus, it seems that the incorporation of three LNA nucleotides changes the structure of the DNA strand completely (except for the terminal nucleotides).

The CD spectra of duplexes **1**, **2** and **3** agree perfectly with the structural changes described above. With duplex **2**, the spectrum has slightly more *A*-type characteristics than duplex **1**, consistent with a shift of the DNA strand conformation towards an *A* type in the vicinity of the modified nucleotide. The spectrum of duplex **3** shows exclusively *A*-type characteristics, consistent with a duplex structure in which both strands adopt sugar conformations corresponding to the standard *A*-type duplex structure.

Stability: Formation of a duplex from two single-stranded nucleic acids is highly unfavourable entropically owing to the concomitant loss of rotational and translational degrees of freedom along with the freezing out of internal bond rotations. Helix formation is a spontaneous reaction only because of a very favourable enthalpy term stemming from base stacking and hydrogen bonding. Searle and Williams[36] have discussed the stability of nucleic acid structures in solution in terms of enthalpy – entropy compensations; following their outline, the effect of introducing a modification can be explained by a change of the free energy of the "internal rotors" of the phosphate backbone (ΔG_r) and the free energy related to the base stacking (ΔG_s). The change of the free energy of the base stacking is dominated by an enthalpy change ($\Delta G_s \approx \Delta H_s$), whereas the change of the free energy of the internal rotors of the backbone is dominated by entropy.[36]

Previously,[24] we investigated the conformation of the single-stranded oligonucleotide d(C$\mathbf{T^L}$GA$\mathbf{T^L}$A$\mathbf{T^L}$GC) (ssLNA) and the corresponding LNA:DNA duplex d(C$\mathbf{T^L}$GA$\mathbf{T^L}$A$\mathbf{T^L}$GC):d(GCATATCAG). We found that the ssLNA strand is to some degree preorganized so that a smaller change of backbone entropy (ΔS_r) has to occur upon the duplex formation. We suggested that the local change of the phosphate backbone geometry in LNA-modified duplexes favours a higher degree of stacking and hence an increased value of $-\Delta H_s$.

The stability of partly modified LNA:RNA duplexes can be explained in exactly the same way: The locked C3′-*endo* conformation of the LNA nucleotide locally organizes the phosphate backbone (decreased loss of entropy upon duplex formation) in the direction of a conformation that in the duplex favours a more efficient stacking of the nucleobases (increased loss in enthalpy upon formation). Thus, the formation of an LNA:RNA duplex is favoured both enthalpically and entropically over formation of the corresponding DNA:RNA duplex.

Implications for RNase H activity: The modus operandi of RNase H has yet to be fully understood. However, the capability of the enzyme to discriminate between DNA:DNA and DNA:RNA duplexes as substrates is well elucidated.[8, 9] A minor groove width intermediate between that of DNA:DNA (*B*-form) duplexes and RNA:RNA (*A*-form) duplexes is proposed as the key recognition element in the ability of RNase H to distinguish substrates from nonsubstrates.[9]

A duplex of partly modified LNA and complementary RNA has been shown to induce RNase H cleavage.[37] Therefore, the pertinent question is: How many LNA modifications in an LNA:RNA duplex are possible while the requirement that the overall duplex geometry be intermediate between *A* and *B* form is still fulfilled? The conformational changes observed in duplex **2** suggest that the LNA nucleotide perturbs only flanking nucleotides, with the 3′-flanking nucleotide changed completely to an *N*-type sugar conformation. Still, the *A*-type conformation of the $\mathbf{T^L}$2-G3-A4-$\mathbf{T^L}$5 segment in duplex **3** suggests that replacing every third nucleotide with an LNA-modified nucleotide would shift the conformation of the duplex completely to the *A* form. This cooperative effect when several LNA modifications are incorporated in a DNA strand is reflected in the fact that the increase per modification in the melting temperature is smaller for fully modified duplexes than for partly modified duplexes.[10, 11, 13] Then, perhaps, as in the case of the 2′-*O*-alkylribose modification,[38] only every fourth or fifth nucleotide should be modified? It should be kept in mind that even this sparse modification of a DNA strand would yield a substantial increase in duplex stability. To counter exonucleolytic degradation, phosphorthioate modifications could also be introduced, since it has been demonstrated that chimeric phosphorthioate–LNA retains the excellent hybridization ability of LNA.[16] However, biological experiments, some of which are already under way, are needed to resolve our questions.

Experimental Section

Sample preparation: The oligonucleotides were synthesized as described elsewhere[10, 11] and purified by filtration through a Sephadex G-15 column. On the basis of 1-D ^{1}H NMR spectra and capillary gel electrophoresis, the oligonucleotides were assessed as containing less than 5% impurities. NMR samples were obtained by dissolving equimolar amounts of the two single strands in 0.5 mL of 10 mM sodium phosphate buffer (pH 7.0), 100 mM NaCl and 0.05 mM EDTA. For experiments carried out in D_2O the solid duplexes, lyophilized twice from D_2O, were redissolved in 99.96% D_2O (Cambridge Isotope Laboratories). A mixture of 90% H_2O and 10% D_2O (0.5 mL) was used for experiments examining exchangeable protons. The final concentrations of the duplexes were 0.7–2.0 mM.

NMR experiments: DQF COSY and TOCSY spectra of the duplexes were recorded on a Varian Unity 500 spectrometer at 25 °C. DQF COSY spectra were obtained with a pulse sequence in which the first pulse was replaced with an E-BURP type selective pulse.[39] The spectra were recorded with a spectral width of 5000 Hz in F_2 and 1000 Hz in F_1 with the States phase cycling scheme with 2048 complex points in t_2. The residual signal from HOD was removed by presaturation.

NOE buildups of duplexes **1** and **3** were obtained on a Varian Inova 750 spectrometer at 25 °C. These spectra were acquired in D_2O using 2048 complex points in t_2 and 512 t_1 experiments with a repetition delay of 3.7 s. NOESY spectra with mixing times of 60, 120, 200 and 300 (**1** only) ms were obtained sequentially without removing the sample from the magnet. The residual signal from HOD was removed by presaturation. Furthermore, an inversion recovery experiment was performed in each case. NOE buildups of duplex **2** were obtained on a Varian Unity 500 spectrometer at 25 °C with experimental conditions as described above. The mixing times used in this case were 100, 200 and 300 ms.

Watergate NOESY spectra in H_2O were acquired on a Varian Inova 750 spectrometer at 25 °C with mixing times of 200 ms.

The acquired data were processed by Felix (version 97.2, MSI/Biosym Technologies, San Diego). All spectra were apodized by a skewed sine bell squared in F_1 and F_2. The NOESY spectra recorded in the buildups of duplexes **1** and **3** and the NOESY spectra recorded in H_2O were linear-predicted from 256 points to 512 points, zero-filled to 2 K points in F_1 and baseline-corrected in F_2 by means of the FLATT routine.[40]

Interproton distances: The upper and lower diagonal parts of each of the NOESY buildup spectra were integrated separately with FELIX, yielding eight, six and six peak intensity sets for duplexes **1**, **2**, and **3**, respectively. The integrated peak intensities were corrected for saturation effects using T_1 relaxation times obtained from inversion recovery experiments. The RANDMARDI procedure[32] of the complete relaxation matrix analysis method MARDIGRAS[31] was used to calculate interproton distances from the peak intensity sets. In the calculations, an absolute noise level of the same order of magnitude as the smallest integrated cross-peak was used for each duplex. A relative integration error for each peak was set at 10% of the integrated peak intensity throughout the calculations. The dynamic ranges of observed cross-peak intensities were between 5000 and 30000 in the various spectra. In the RANDMARDI procedure, 30 different intensity sets were generated from each experimental data set based on the given noise levels, and MARDIGRAS calculations were performed on all of them. The distances resulting from all generated intensity sets were combined into a single distance file for each duplex.

Deoxyribose ring conformations: The H1′ to H2′ and H2″ region of the selective DQF COSY spectra was used as input to CHEOPS[34] to obtain the values of the *J* coupling constants for the H1′, H2′, H2″ and H3′ deoxyribose ring protons[34, 41]. The deoxyribose ring conformations were analyzed assuming a fast two-state equilibrium between *N*- and *S*-type conformations with a modified version of the program PSEUROT.[35] The standard version of PSEUROT applies a least-squares optimization routine to obtain the best fit of the parameters P_N, P_S, $I_{max,N}$, $I_{max,S}$ and $\%N$ to the experimental coupling constants. $P_{N,S}$ and $I_{N,S}$ are the pseudorotation angle and puckering amplitude, respectively, of the *N*- and *S*-type conformation and $\%N$ is the mole fraction of the *N*-type conformation. In our randomized version of PSEUROT (RANDPSEUROT), we include the effect of uncertainties in the determined set of coupling constants. RANDPSEUROT generates 1000 sets of coupling constants by adding a random number to each experimentally determined coupling constant. The random numbers are generated according to a normal distribution[42] in which the dispersion is set according to the uncertainty of each determined coupling constant. Uncertainties of the coupling constants are carefully assessed by how well the back-calculated spectrum correlates with the experimental spectrum and by the response of the determined coupling constants to small changes in the simulation procedure. Subsequently, PSEUROT calculations are executed for all the generated sets of coupling constants and RANDPSEUROT then calculates mean values and standard deviations of the parameters returned by PSEUROT. In the statistical analysis, *N*-type conformations are compared with *N* types and *S*-type conformations are compared with *S* types based on the parameters returned by PSEUROT. In cases where PSEUROT returns either two *N*-type or two *S*-type conformations the two conformations are sorted according to the major conformer.

Thermal stability studies: The thermal stabilities of the duplexes were determined spectrophotometrically by means of a spectrophotometer equipped with a thermoregulated Peltier element. Hybridization mixtures were prepared by dissolving equimolar (2.4–2.7 μM) amounts of the oligonucleotides in 10 mM sodium phosphate buffer (pH 7.0), 100 mM NaCl and 0.05 mM EDTA. The absorbance at 260 nm was monitored while the temperature was raised linearly from 10–80 °C (1 °C min^{-1}). The melting temperatures (T_m values) were obtained as the maxima of the first derivative of the melting curves.

Circular dichroism spectra: CD spectra of the duplexes from 350 to 200 nm were measured on a Jasco710/720. Solutions were prepared by dissolving

0947-6539/00/0615-2694 $ 17.50+.50/0 *Chem. Eur. J.* **2000**, *6*, No. 15

equimolar (40–80 μM) amounts of the oligonucleotides in 10 mM sodium phosphate buffer (pH 7.0) and 0.05 mM EDTA. The spectrum of the buffer solution was subtracted from each spectrum. The molar CD of the duplexes was calculated from Equation (1),[43, 44] where θ is the measured ellipticity

$$\Delta\varepsilon = \frac{\theta}{32.98\, C\, L} \quad (1)$$

in degrees, L is the path length in centimeters, and C is the concentration of the duplexes. Absorbance spectra of the solutions were measured on a Lambda 17 spectrophotometer. Concentrations of the duplexes were determined from the absorbance at 260 nm using an extinction coefficient $\varepsilon = 161\,800\ \mathrm{M^{-1}\,cm^{-1}}$.

Acknowledgements

We thank Dr. Thomas Franch and Dr. Inge D. Villsen (Department of Molecular Biology, University of Southern Denmark) for help in handling the RNA. We are also grateful to Dr. Svend Erik Harnung and Karen Jørgensen (Department of Chemistry, University of Copenhagen) for recording the CD spectra. We thank the Instrument Center for NMR Spectroscopy of Biological Macromolecules at the Carlsberg Laboratory, Copenhagen (recipient of a grant from the Danish Natural Science Research Council) for providing spectrometer time at the 750 MHz spectrometer. Finally, financial support from the Danish Natural Science Research Council and the Technical Research Council are acknowledged.

[1] C. Hélène, J.-J. Toulmé, *Biochem. Biophys. Acta* **1990**, *1049*, 99–125.
[2] E. Uhlmann, A. Peyman, *Chem. Rev.* **1990**, *90*, 543–584.
[3] C. Hélène, *Anti-Cancer Drug Design* **1991**, *6*, 569–584.
[4] N. T. Thuong, C. Hélène, *Angew. Chem.* **1993**, *105*, 697–723; *Angew. Chem. Int. Ed. Engl.* **1993**, *32*, 666–690.
[5] P. E. Nielsen, *Bioconjugate Chem.* **1991**, *2*, 1–12.
[6] A. De Mesmaeker, R. Häner, P. Martin, H. E. Moser, *Acc. Chem. Res.* **1995**, *28*, 366–374.
[7] W. F. Flanagan, *Cancer Metastasis Rev.* **1998**, *17*, 169–176.
[8] O. Y. Fedoroff, M. Salazar, B. R. Reid, *J. Mol. Biol.* **1993**, *233*, 509–523.
[9] J.-J. Toulmé, D. Tidd in *Ribonucleases H* (Eds.: R. J. Crouch), ISERM, Paris, **1998**, pp. 225–250.
[10] A. A. Koshkin, S. K. Singh, P. Nielsen, V. K. Rajwanshi, R. Kumar, M. Meldgaard, C. E. Olsen, J. Wengel, *Tetrahedron* **1998**, *54*, 3607–3630.
[11] S. K. Singh, P. Nielsen, A. A. Koshkin, J. Wengel, *Chem. Commun.* **1998**, 455–456.
[12] S. K. Singh, J. Wengel, *Chem. Commun.* **1998**, 1247–1248.
[13] J. Wengel, *Acc. Chem. Res.* **1998**, *32*, 301–310.
[14] A. A. Koshkin, P. Nielsen, M. Meldgaard, V. K. Rajwanshi, S. K. Singh, J. Wengel, *J. Am. Chem. Soc.* **1998**, *120*, 13252–13253.
[15] S. Obika, D. Nanbu, Y. Hari, K. Morio, Y. In, T. Ishida, T. Imanishi, *Tetrahedron Lett.* **1997**, *38*, 8735–8739.
[16] R. Kumar, S. K. Singh, A. A. Koshkin, V. K. Rajwanshi, M. Meldgaard, J. Wengel, *Biorg. Med. Chem. Lett.* **1998**, *8*, 2219–2222.
[17] J. Wengel, A. Koshkin, S. K. Singh, P. Nielsen, M. Meldgaard, V. K. Rajwanshi, R. Kumar, J. Skouv, C. B. Nielsen, J. P. Jacobsen, N. Jacobsen, C. E. Olsen, *Nucleosides Nucleotides* **1999**, *18*, 1365–1370.
[18] R. E. Dickerson, M. Bansal, C. R. Calladine, S. Diekmann, W. N. Hunter, O. Kennard, E. von Kitzing, H. C. M. Nelson, R. Lavery, W. K. Olson, W. Saenger, Z. Shakked, D. M. Soumpasis, C.-S. Tung, H. Sklenar, A. H. J. Wang, V. B. Zhurkin, *EMBO J.* **1989**, *8*, 1–4.
[19] W. Saenger, *Principles of Nucleic Acid Structure*, Springer, New York, **1984**.
[20] C. Altona, M. Sundaralingam, *J. Am. Chem. Soc.* **1972**, *94*, 8205–8212.
[21] C. Altona, M. Sundaralingam, *J. Am. Chem. Soc.* **1973**, *95*, 2333–2344.
[22] W. K. Olson, J. L. Sussman, *J. Am. Chem. Soc.* **1982**, *104*, 270–278.
[23] K. A. Brameld, W. A. Goddard III, *J. Am. Chem. Soc.* **1999**, *121*, 985–993.
[24] M. Petersen, C. B. Nielsen, K. E. Nielsen, G. A. Jensen, K. Bondensgaard, S. K. Singh, V. K. Rajwanshi, A. A. Koshkin, B. M. Dahl, J. Wengel, J. P. Jacobsen, *J. Mol. Recognit.* **2000**, *13*, 44–53.
[25] C. B. Nielsen, S. K. Singh, J. Wengel, J. P. Jacobsen, *J. Biomol. Struct. Dyn.* **1999**, *17*, 175–191.
[26] K. E. Nielsen, S. K. Singh, J. Wengel, J. P. Jacobsen, *Bioconjugate Chem.* **1999**, in press.
[27] D. R. Hare, D. E. Wemmer, S.-H. Chou, G. Drobny, B. R. Reid, *J. Mol. Biol.* **1983**, *171*, 319–336.
[28] K. Wüthrich, *NMR of Proteins and Nucleic Acids*, John Wiley, New York, **1986**.
[29] J. Feigon, W. Leupin, W. A. Denny, D. R. Kearns, *Biochemistry* **1983**, *22*, 5943–5951.
[30] R. M. Scheek, N. Russo, R. Boelens, R. Kaptein, *J. Am. Chem. Soc.* **1983**, *105*, 2914–2916.
[31] B. A. Borgias, T. L. James, *J. Magn. Reson.* **1990**, *87*, 475–487.
[32] H. Liu, H. P. Spielmann, N. A. Ulyanov, D. E. Wemmer, T. L. James, *J. Biol. NMR* **1995**, *6*, 390–402.
[33] U. Schmitz, T. L. James, *Methods Enzymol.* **1995**, *261*, 3–44.
[34] R. F. Macaya, P. Schultze, J. Feigon, *J. Am. Chem. Soc.* **1992**, *114*, 781–783.
[35] F. A. A. M. de Leeuw, C. Altona, *J. Comput. Chem* **1983**, *4*, 428–437.
[36] M. S. Searle, D. H. Williams, *Nucleic Acid Res.* **1993**, *21*, 2051–2056.
[37] C. Wahlestedt, P. Salmi, L. Good, J. Kela, T. Johnsen, T. Hökfelt, C. Broberger, F. Porreca, A. Koshkin, M. H. Jacobsen, J. Wengel, **1999**, *Proc. Natl. Acad. Sci. USA* **2000**, *97*, 5633–5638.
[38] H. Wu, W. F. Lima, S. T. Crooke, *J. Biol. Chem.* **1999**, *274*, 28270–28278.
[39] H. Geen, R. Freeman, *J. Magn. Reson.* **1991**, *93*, 93–141.
[40] P. Güntert, K. Wüthrich, *J. Magn. Reson.* **1992**, *96*, 403–407.
[41] M. Gochin, G. Zon, T. L. James, *Biochemistry* **1990**, *29*, 11161–11171.
[42] W. H. Press, B. P. Flannery, S. A. Teukolsky, W. T. Vetterling, *Numerical Recipes*, Cambridge University Press, Cambridge, **1986**.
[43] R. W. Woody, *Methods Enzymol.* **1995**, 34–71.
[44] W. A. Baase, W. C. Johnson, *Nucleic Acid Res.* **1979**, *6*, 797–814.

Received: November 9, 1999 [F2128]